

Scanning laser reflection tool for alignment and period measurement of critical-angle transmission gratings

Jungki Song,¹ Ralf K. Heilmann,¹ Alexander R. Brucoleri,² Edward Hertz,³ and Mark L. Schattenburg¹

¹Space Nanotechnology Laboratory, MIT Kavli Institute for Astrophysics and Space Research, Massachusetts Institute of Technology, Cambridge, Massachusetts 02139, USA

²Izentis LLC, PO Box 397002, Cambridge, MA 02139, USA

³Harvard-Smithsonian Center for Astrophysics, Cambridge, MA, USA

ABSTRACT

We report progress toward developing a scanning laser reflection (LR) tool for alignment and period measurement of critical-angle transmission (CAT) gratings. It operates on a similar measurement principle as a tool built in 1994 which characterized period variations of grating facets for the *Chandra X-ray Observatory*. A specularly reflected beam and a first-order diffracted beam were used to record local period variations, surface slope variations, and grating line orientation. In this work, a normal-incidence beam was added to measure slope variations (instead of the angled-incidence beam). Since normal incidence reflection is not coupled with surface height change, it enables measurement of slope variations more accurately and, along with the angled-incidence beam, helps to reconstruct the surface figure (or tilt) map. The measurement capability of in-grating period variations was demonstrated by measuring test reflection grating (RG) samples that show only intrinsic period variations of the interference lithography process. Experimental demonstration for angular alignment of CAT gratings is also presented along with a custom-designed grating alignment assembly (GAA) testbed. All three angles were aligned to satisfy requirements for the proposed Arcus mission. The final measurement of roll misalignment agrees with the roll measurements performed at the PANTER x-ray test facility.

1. INTRODUCTION

A number of high-priority questions in astrophysics can be addressed by high-resolution x-ray spectroscopy. However, grating spectrometers used in *Chandra* and *XMM-Newton* are outdated, and realization of an x-ray grating spectrometer (XGS) that promises both large collecting area and high resolving power (e.g. the *Arcus* mission¹ proposed as a MIDEX) is still a challenge. Critical-angle transmission (CAT) gratings, with the combined advantages of blazed reflection gratings and conventional transmission gratings, are expected to lessen the hurdles to fulfill aforementioned requirements—they have more relaxed alignment tolerances, high diffraction efficiency, and require fewer gratings to cover large telescope apertures.² The fabrication process for CAT gratings is described elsewhere.³⁻⁷ It was demonstrated that diffraction from a single CAT grating facet in a spectrometer (nominal period of 200 nm) can achieve high resolving power ($\lambda/\Delta\lambda$) of >10,000 in 18th diffraction order at Al K α wavelength.⁸ Period variation is the main potential limiting factor to achieve very high resolving power. A fast method for precise grating period measurement in air will provide important quality control during the production of large arrays of gratings and eliminate the need for time-consuming x-ray characterization. Likewise, alignment methodology for multiple CAT grating facets needs to be developed to achieve large collecting area.

Prior to developing a metrology system for CAT gratings, we revisited the metrology system used for measurement of period variations and angular misalignments of transmission gratings for the *Chandra* x-ray telescope.^{9,10} Fig. 1a shows a schematic of the laser reflection (LR) tool which characterized *Chandra* HETGS grating period variations two decades ago.⁹ The tool raster-scanned the grating surface with an angled-incidence beam and measured the change of position of a specularly reflected beam and a first-order diffracted beam to record local period variations, surface slope variations, and grating line orientation. However, it is unclear how authors compensated for measurement errors due to surface height change (i.e., height change due to tilt error or distortion of the grating). For grating alignment, authors used the partial

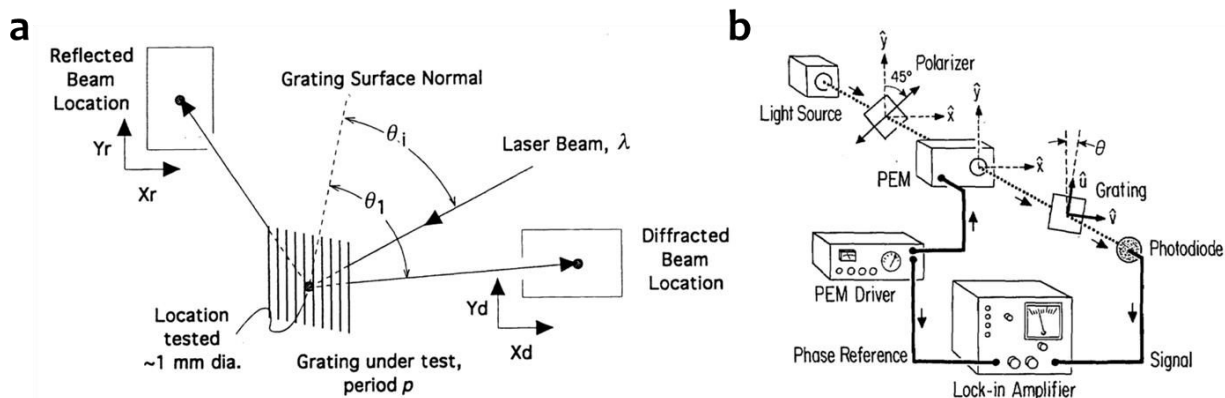


Figure 1. **a**, Schematic of *Chandra*-era laser reflection (LR) period mapping tool. **b**, Polarization-based roll alignment system built for the *Chandra* x-ray telescope.

polarization property of fine-pitched transmission gratings.¹⁰ Fig. 1b shows a schematic of the metrology system used to align multiple grating facets for *Chandra*. A photoelastic modulator and lock-in amplifier was used to “detect a signal proportional to the sine of twice the angle between the grating lines and the axis of the PEM” for alignment.¹⁰ However, this alignment technique could be of limited use for CAT gratings due to structural differences;² for example, parasitic partial polarization from the integrated cross-support mesh (L1) and stress birefringence in the buried oxide layer have the potential to degrade the accuracy of this method.

We added a normal-incidence beam to the scanning LR tool to allow measurement of both period and angular misalignments. Unlike the angled-incidence beam for which the position of both reflected and back-diffracted beams are affected by surface height change – be it from surface topography or scanning across a tilted grating, a normal incidence beam is not coupled with surface height variations, enabling generation of more accurate surface slope maps. After aligning both beams to the same position on the grating surface, surface height variations (or tilt error), period variations, and grating line roll variations were measured across the test grating sample (see Sect. 3). Accurate measurement of slope variations enables the tool to be used as an angular metrology system for alignment of CAT gratings as well. The normal-incidence and back-diffracted beams were used to measure yaw, pitch, and roll variations as we scan along a line across multiple gratings, and all three angles were aligned to satisfy Arcus mission requirements.¹¹

This paper is organized as follows: Sect. 2 discusses the newly developed scanning LR tool. In Sect. 3, measurement capability of detecting in-grating period variations for a test reflection grating (RG) is shown. In Sect. 4, a first demonstration of CAT grating alignment is presented.

2. EQUIPMENT SETUP

The scanning LR tool has five main components: a 325 nm HeCd laser source, a high-precision XY stage, a 3-axis rotation stage, a grating mount, and three position-sensitive detectors (PSDs). The beam from the UV laser is split into two beams, which are reflected by mirrors (or beam splitter) to be incident upon the same spot on the grating with different incidence angles (60° and 0° for the angled-incidence and normal-incidence beams, respectively). The angled beam was partially masked so that the projected beam forms a similar (approximately circular) shape as the normal-incidence beam on the grating. The diameter of the incident beams can be adjusted to be 0.25-1 mm using pairs of focusing lenses. Fig. 2 shows a schematic and photograph of the tool. Coordinate systems for detectors and grating (Fig. 2a), incidence/back-diffracted angles (θ_i, θ_d) and path lengths for angled-reflected, normal-reflected, and back-diffracted beams (R_R, R_N, R_D) (Fig. 2b) are shown. PSDs find the center of mass of beams with sampling frequency of 1000 Hz averaged for 2 seconds. A 3-axis rotation stage is used to reduce grating tilt error (yaw, pitch) about the axes of the raster scan and characterize the correction factor for yaw for period mapping.

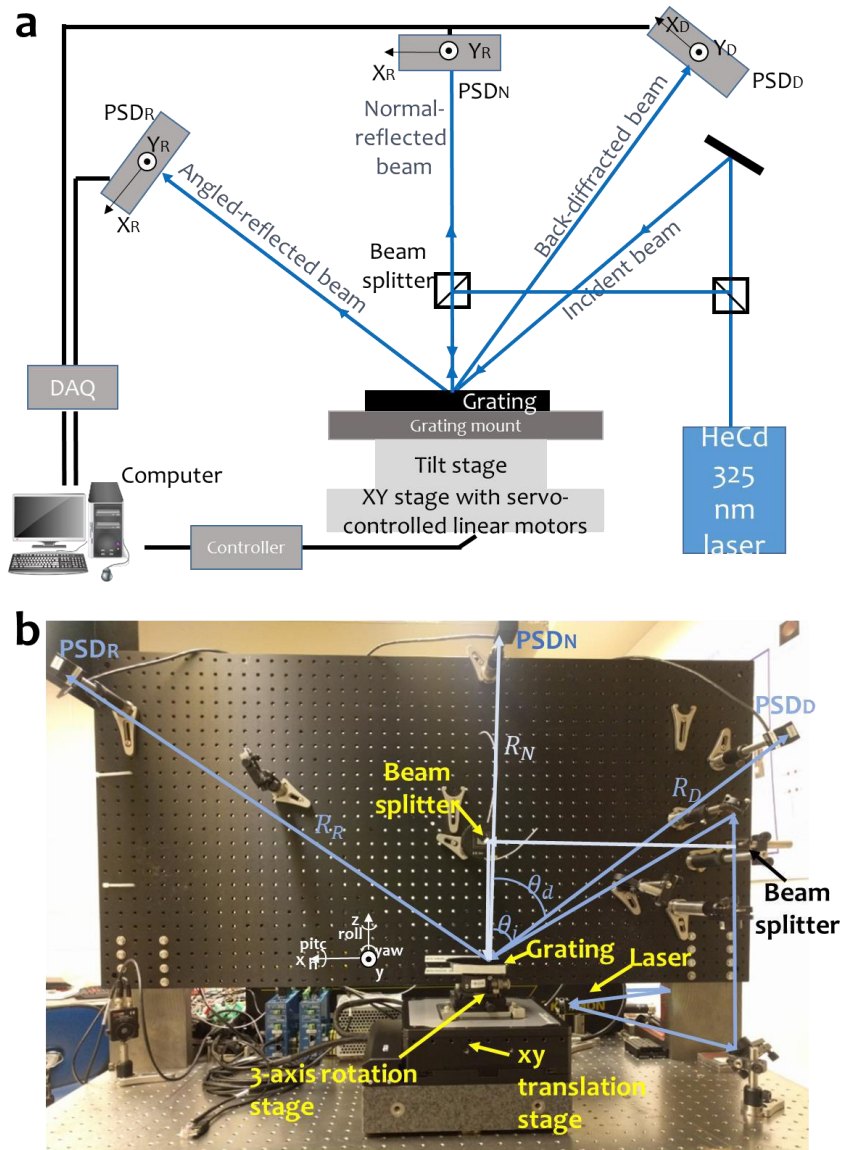


Figure 2. Laser reflection (LR) tool for measurement of angular misalignments and period variations. **a**, Schematic of the modified LR tool. Coordinate systems for detectors and grating are shown. **b**, LR Tool for angular alignment and period mapping. Angles and beam path lengths are also shown.

Detector position measurement noise was measured to be less than $\pm 0.58 \mu\text{m}$ rms with corresponding period measurement error of $4.2 \times 10^{-4} \text{ nm}$. Overall period measurement repeatability was calibrated by measuring the same area ($50 \text{ mm} \times 60 \text{ mm}$, 1 mm interval) of a single test reflection grating (RG) sample for 3 times (the test RG was remounted between the measurements), and is estimated to be 20 ppm rms (compared to 40 ppm rms for the *Chandra* LR tool). Measurement repeatability of angular misalignments between the CAT gratings was determined by scanning along line A-A' (see Fig. 6 in Sect. 4) for 3 times on different days (the grating alignment assembly was remounted between the measurements), and it was found to be 0.06, 0.11, and 0.67 arc min rms for yaw, pitch, and roll, respectively. Based on conservative error analysis, total errors are estimated to be ± 0.1 , ± 0.8 , and ± 1.1 arc min for yaw, pitch, and roll, respectively.

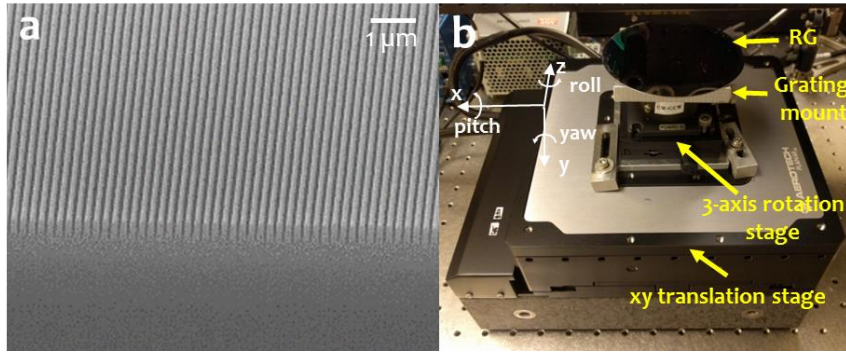


Figure 3. **a**, SEM image of cleaved RG with 200-nm pitch. **b**, RG mounted on the grating mount.

3. SYSTEM CALIBRATION FOR PERIOD MEASUREMENTS

3.1. Test reflection grating sample preparation

Test RGs with nominally 200 nm pitch, and built-in period variations due to spherical wave interference during patterning¹² were used to demonstrate measurement capability of small period variations. The 100 mm-diameter silicon wafers were patterned via interference lithography on a Mach-Zehnder interferometer, and etched approximately 500 nm via reactive-ion etching. After etching, the samples were cleaned of all organic materials via a mixture of sulfuric acid and hydrogen peroxide followed by a heated mixture of diluted peroxide and ammonium hydroxide. Fig. 3a shows a SEM image of a cleaved test RG. The fabricated RGs were bonded on the grating mount with three contact points, and a drop of acetone was used to release it after measurements. Fig. 3b shows a RG mounted on the stage including the wafer coordinate system.

3.2. Calibration

Path lengths for all three beams (R_R, R_N, R_D), and angles of incident and back-diffracted angles (θ_i, θ_d), were measured using a ruler and fluorescent card, respectively. After aligning all three beams to be in-plane, a fluorescent card was placed along the same plane, and images of fluorescent laser paths were captured and analyzed to calibrate angles. The correction factor for yaw was calibrated by yawing the stage while recording the rate of change of normal-reflected and back-diffracted beams (see Eqns. 1, 5 in next Section).

3.3 Period mapping

The test RG was raster-scanned in 1-mm intervals to record period variations (dp), grating surface slope variations ($dYaw, dPitch$), grating line rotation ($dRoll$), and surface height change (dz). The grating period at the center of the wafer was assumed to be 200 nm and was used as a reference (a reference grating with a well calibrated period will be mounted on the stage in future). Unlike the LR tool built for the *Chandra* x-ray telescope, surface slope variations were measured using the normal-reflected beam and, along with the angled-reflected beam, the surface figure (or tilt) map was reconstructed. The modified set of equations is as follows:

$$dX_N = 2R_N dYaw \quad (1)$$

$$dY_N = -2R_N dPitch \quad (2)$$

$$dX_R = 2R_R dYaw - 2 \sin \theta_i dz \quad (3)$$

$$dY_R = -2R_R \cos \theta_i \cdot dPitch + 2dz \cdot dPitch \quad (4)$$

$$dX_D = R_D \left(\frac{\cos \theta_d + \cos \theta_i}{\cos \theta_d} \right) dYaw + R_D \frac{dp}{p} \frac{(\sin \theta_d + \sin \theta_i)}{(\cos \theta_d)} - \frac{dz}{\cos(\theta_i)} \sin(\theta_i - \theta_d) \quad (5)$$

$$dY_D = -R_D (\cos \theta_d + \cos \theta_i) dPitch - R_D (\sin \theta_d + \sin \theta_i) dRoll + dz \left(\left(1 + \frac{\cos \theta_i}{\cos \theta_d} \right) dPitch + \left(\tan \theta_d + \frac{\sin \theta_i}{\cos \theta_d} \right) dRoll \right) \quad (6)$$

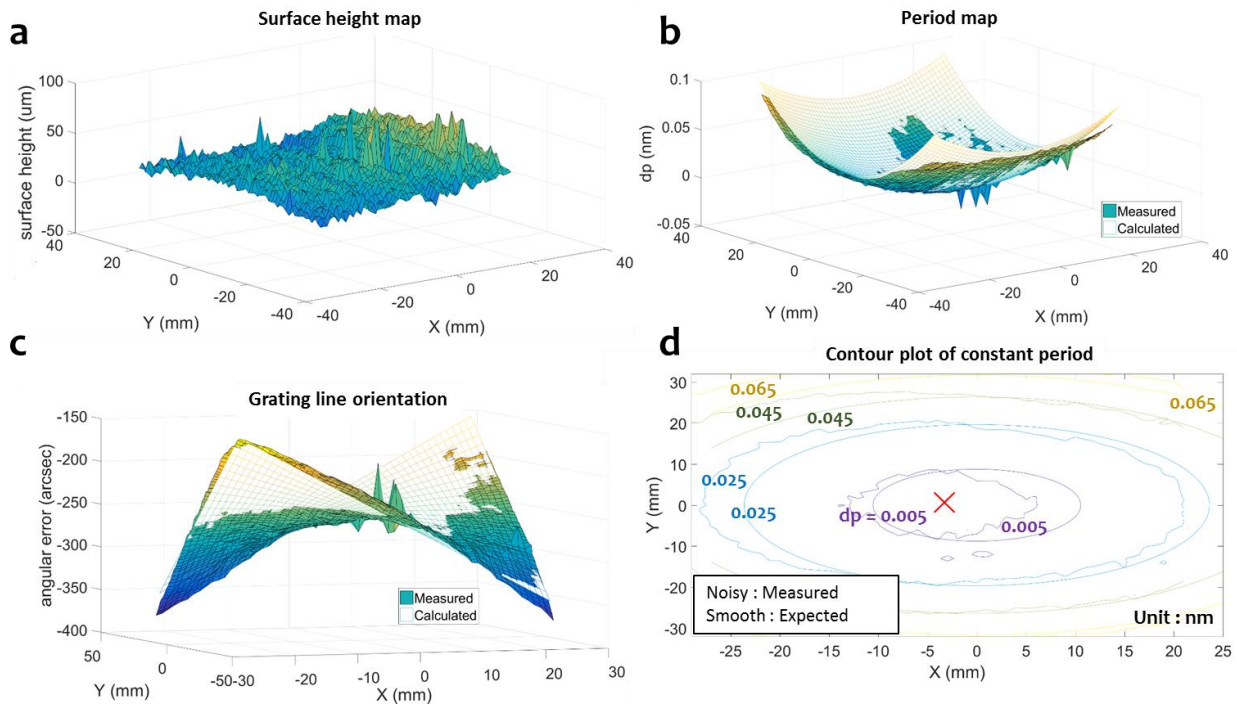


Figure 4. **a**, Measured surface figure (or tilt) map of RG in 3D space. **b**, Calculated and measured period variations of RG. The two plots were centered at (0,0) for comparison. **c**, Calculated and measured variations of grating line orientation of RG. The two plots were centered at (0,0) for comparison. **d**, Measured (noisy) and theoretical (smooth) contour maps of constant period for RG. Unlike Fig. 4b, measured data were not centered. The offset between the center of the theoretical and measured data indicates that the interference pattern during resist exposure was not precisely centered in the middle of the wafer. Red 'X' located at (-4,0) on wafer substrate indicates the center of measured contour map. Spikes in 3D graphs are due to scratch on the surface of the RG.

where $dX_N, dY_N, dX_R, dY_R, dX_D, dY_D$ indicate change of positions on each detector in x & y direction (see detector coordinates in Fig. 2a). $dYaw, dPitch, dRoll, R_N, R_D, R_R, \theta_i, \theta_d$ are indicated in Fig. 2b, and dz indicates change of surface height.

Eqns. 1-2 explain the position change of the normal-reflected beam as a function of surface slope (yaw, pitch). Eqns. 3-6 are similar to those derived in Dewey D. *et al.*⁹ except that the surface height change (dz) was taken into account. Eqns. 1-2 were used to map the surface slope variations (yaw, pitch), Eqns. 1, 3 to reconstruct the surface height variations (dz) in 3D space, Eqns. 1, 5 for period variations (dp), and Eqns. 2, 6 for grating line rotation ($dRoll$). It should be noted that tilt errors (yaw, pitch) of the grating surface were minimized prior to measurements to minimize the effect of surface height changes (3rd term in Eqn. 5).

Fig. 4a shows a surface figure map, indicating the surface of the grating is leveled with the raster-scan plane. The $<50 \mu\text{m}$ P-V is due to a combination of non-flatness of the test grating sample and potential stage errors. Fig 4b shows measured and expected period variations of the RG. Theoretically expected values of period variation were calculated based on a spherical wave interference model^{12, 13}, and it shows good agreement with measured period variations. Fig. 4c shows measured and expected roll variations for the RG. Both measured and expected grating line orientations show hyperbolic distortion with good agreement. Fig. 4d shows measured (noisy) and theoretical (smooth) contour maps of constant RG period. It implies the center of interference was displaced by (-4,0) mm relative to the wafer center when the grating lines were patterned with the Mach-Zehnder interferometer. The interference pattern has to be well-centered on the substrate to minimize degradation of resolving power since the period varies more rapidly with increasing distance from the wafer center (a rectangular area at the wafer center is used to fabricate CAT gratings).

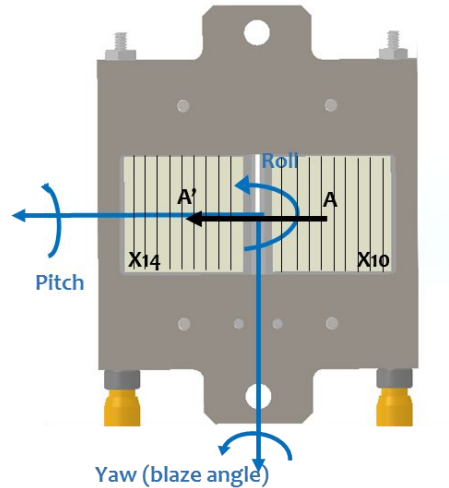


Figure 6. Definition of orientation of angles and scanned line A-A' for measurement of angular misalignment.

4. CAT GRATING ALIGNMENT

4.1 Grating alignment assembly testbed and bonding

Fig. 5a shows a schematic of the grating alignment assembly (GAA) testbed designed for proof-of-concept of high-precision adjustment of roll. CAT gratings were bonded at the center of four flexures that run parallel to each edge of the grating to compensate for CTE mismatch between the grating and the titanium support frame. Fig. 5b shows the bonding process for the CAT gratings: 0.012 inch diameter wire was placed between the frame and the grating near each end of the grating to set the bond thickness for attachment to the integral flexure support. The wires were carefully removed after a 24-hour cure at room temperature. The frame was attached to the base plate with fasteners and Belleville washers at the

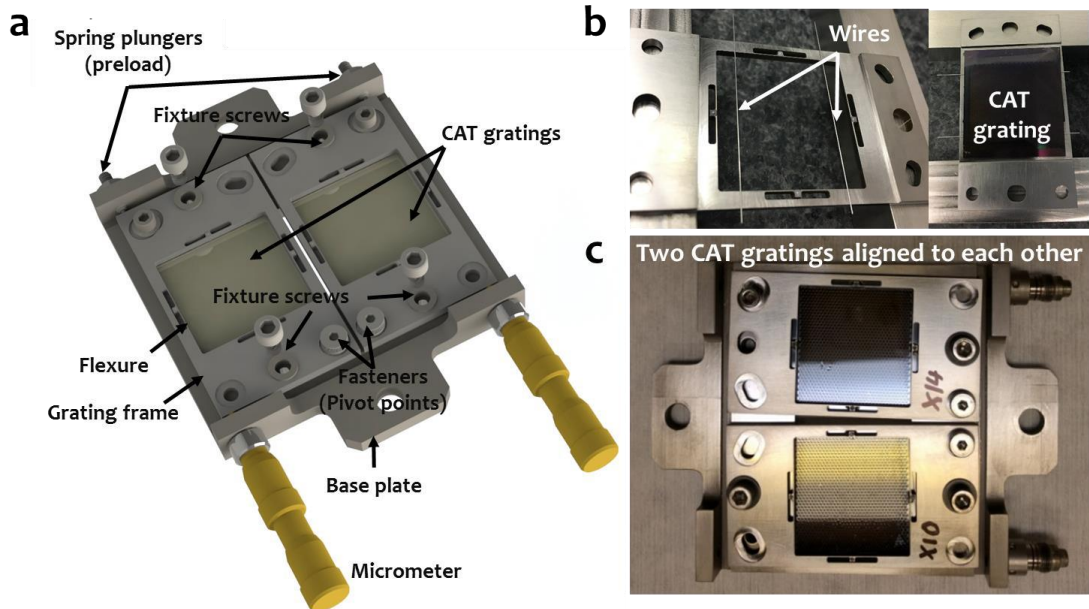


Figure 5. **a**, Schematic of Grating Alignment Assembly indicating components. **b**, bonding process for CAT grating. **c**, grating alignment assembly (GAA) testbed after alignment of two CAT gratings (designated as X10 and X14).

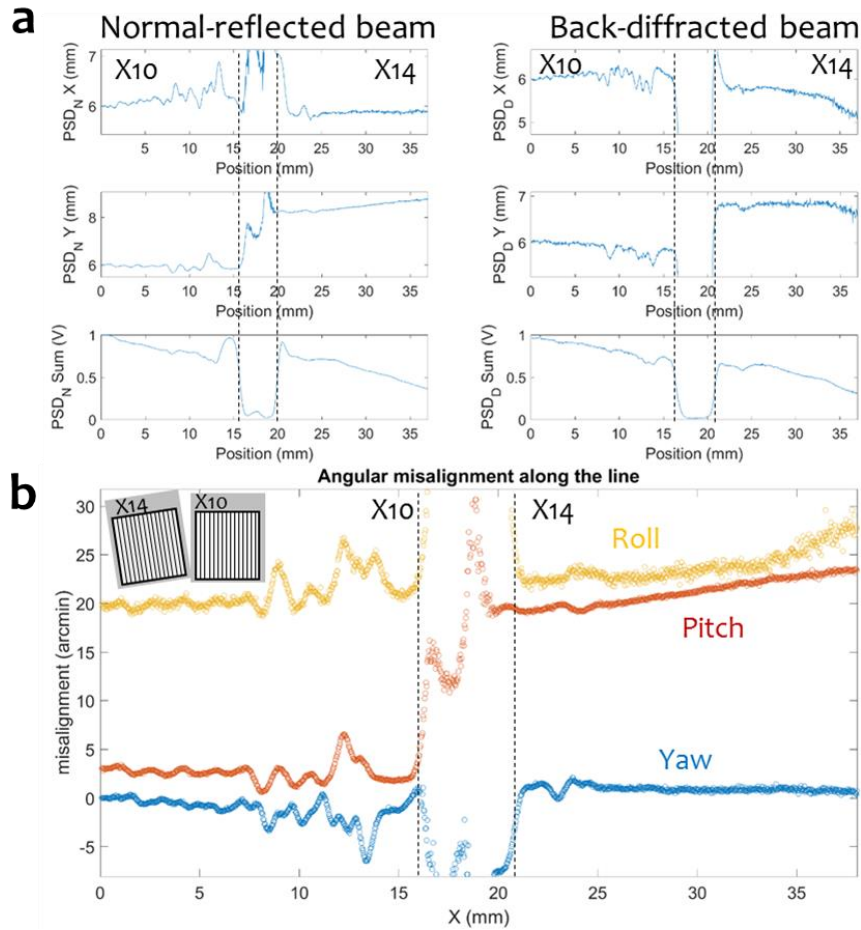


Figure 7. Example measurements (data collected after the GAA testbed was back at MIT) of angular changes along line A-A'. **a**, Change of position in x (the 1st row), and y (the 2nd row) direction of the PSDs. The 3rd row indicates the intensity of the beam. Graphs in the left and right columns are collected from normal-reflected and back-diffracted beams, respectively. **b**, Angle changes along line A-A'. Inset in top left corner schematically shows orientation of roll misalignment for the example data.

pivot point of the CAT gratings. Spring plungers provide pre-load of the frame against the micrometer used for roll adjustments. The fixture screws were tightened once the alignment is complete and requirements have been satisfied. Fig. 5c shows the GAA testbed with the two CAT gratings aligned relative to each other.

4.2 Measurement of angular misalignments

The scanning LR tool was used to scan across line A-A' (see Fig. 6) of two adjacently located CAT gratings to measure variations of angles (yaw, pitch, and roll) along the line. Fig. 7a shows an example of raw data recorded along the line A-A'. The 1st and 2nd rows indicate position changes of the beam in X and Y directions (in detector coordinates, see Fig. 2a for orientation), and the 3rd row indicates the intensity of the beam incident on the detectors. The data between the dotted lines correspond to the gap between the gratings. Angular changes (yaw, pitch, and roll) along the line were derived using Eqns. 1, 2 and 6 (see Fig. 7b). Of note, the 3rd term in Equation 6 was neglected since surface height change effect on roll measurement was negligibly small (2nd order term). Orientation of angles can be found in Fig. 6. Fig. 7b indicates misalignment of X14 relative to X10; i.e., orientation of roll misalignment is visualized in inset at the top left corner as an example.

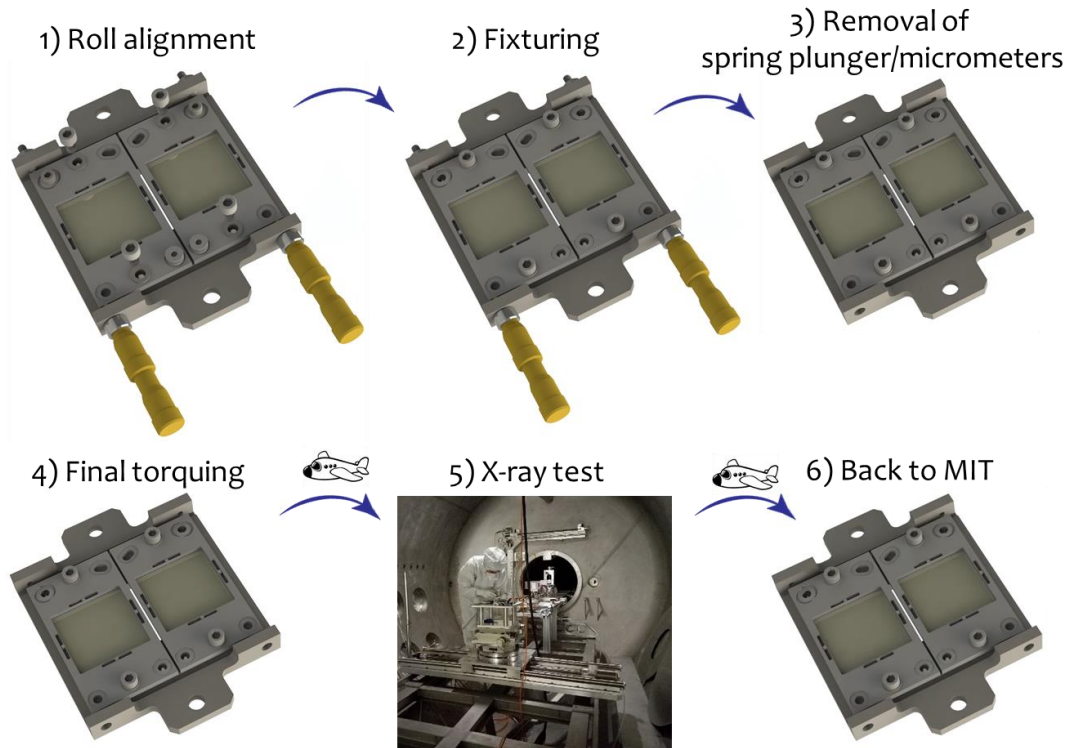


Figure 8. Sequence of roll measurements. Angular misalignments were measured after each step.

4.3 Sequence of roll alignment

We sub-divided the alignment and measured misalignments after each step in order to understand mechanical drifts throughout the process. Measurements were taken before and after trips between the PANTER X-ray Test Facility in Germany and MIT as well. Fig. 8 summarizes the alignment (or travel) log at each step. First, the grating frames were rolled using micrometers for alignment. Preloads were kept small and micrometers were retracted several times during alignment to reduce distortion of the frames. Second, the frames were locked in position with fixture screws and all other fasteners were removed. Third, spring plungers and micrometers were removed. Fourth, the fixture screws were torqued again (3-5 in-lbs) as the last check before packing the grating. Fifth, it was flown to PANTER to measure resolving power and roll alignment.¹⁴ Sixth, it traveled back to MIT. The GAA testbed was packed inside double Ziplock bags in a clean room environment before each travel to prevent contamination.

Table 1 summarizes the measured misalignments after each step. Values indicate line-averaged misalignments of X14 relative to X10 following the orientation shown in Fig. 6. All three angles show drifts in each step, except only roll drifted after removing spring plungers and micrometers. However, drifts of angles were small enough to meet Arcus requirements.¹¹

Table 1. Summary of measurement results after each step.

	Roll alignment	Fixturing	Removal of spring plungers/micrometers	Final torquing	X-ray test	Back to MIT	Arcus requirements [11]
dYaw [arcmin]	-0.9	+2.0	+2.0	+2.5	-	+2.2	± 15 arcmin
dPitch [arcmin]	+8.8	+14.1	+14.0	+10.6	-	+18.5	± 5 deg
dRoll [arcmin]	+3.8	+4.8	+3.4	+0.08	+3.6	+3.3	± 15 arcmin

5 DISCUSSION AND FUTURE PLANS

The scanning LR tool was built to characterize grating period variations and angular misalignments between gratings. Adding a normal-incidence beam allowed more accurate measurement of slope variations, and enabled reconstruction of surface figure maps. The reconstructed surface figure map can be used to characterize slopes of a grating surface relative to the raster-scan plane, investigate non-flatness of the grating, and correct for surface height change when measuring period variations. Offset of the interference pattern from substrate center (measured to be 4 mm for our test grating) can be characterized. The tool was used to align two CAT gratings in the roll direction as well. It measured roll misalignment between two adjacently located CAT gratings with an accuracy of ± 1.1 arc min with a clear path to further improvements (see Sect. 5.2). Two large-area (32 mm \times 32 mm) gratings were successfully aligned to satisfy Arcus mission requirements.

5.1. Issues with period mapping and future plan

While the system can measure period variations of the test RG with high accuracy and has 2X better repeatability as compared to the LR tool built in 1994, it still requires further improvements. Above all, the system needs to measure period variations of CAT gratings, the actual flight hardware. PSDs, which measure the “center of mass” of the beams for position measurements, can generate biased position signals due to the different ‘reflectivities’ for the hexagonal L2 support mesh and grating bars (for structural design of CAT gratings, please refer to Ref. 2). Therefore, the beam has to be positioned on the grating bars (not on the L2 mesh) to prevent biased position measurements. In addition, we are planning to reduce the beam size to resolve the period variations inside single grating membranes (inside the L2 supports).

Another issue that has to be addressed is dimpling of the grating bar membrane inside the hexagonal mesh (L2)². While most of the area does not show dimples, these slight deformations of grating membranes can change the shape of the propagating beam and result in non-Gaussian profiles. This can also lead to bias in position measurements on PSDs. Large-format UV-sensitive image sensors are an option being considered to tackle this problem.

5.2. Issues with grating alignment and future plans

While two CAT gratings were measured to satisfy Arcus requirements, more tests should be performed to determine repeatability. The system needs further improvements in terms of measurement repeatability and accuracy. It was found that the measurement error of beam path length from gratings to detector is a major source of uncertainty, and it could be addressed by using well-calibrated high-resolution goniometric stages (center of rotations for CAT gratings in yaw and pitch direction will be on the same plane); beam path lengths, incident and back-diffracted angles can be characterized with high-accuracy by measuring beam position change on the detectors while rotating the stage by a certain degree. The GAA testbed needs further improvements; frames must get smaller and lighter in weight, it should have less mechanical drift, and the width of the edge cover between the CAT gratings should be reduced.

ACKNOWLEDGEMENTS

This work was supported by NASA grants NNX17AG43G and NNX15AC43G.

REFERENCES

- [1] Smith, R. K. *et al.*, “Arcus: the x-ray grating spectrometer explorer,” *Proc. SPIE* **10397** (paper 41), to be published (2017).
- [2] Heilmann, R. K., Bruccoleri, A. R., and Schattenburg, M.L., “High-efficiency blazed transmission gratings for high-resolution soft x-ray spectroscopy,” *Proc. SPIE* **9603**, 960314-1 (2015).
- [3] Heilmann, R. K. *et al.*, “Fabrication update on critical-angle transmission gratings for soft x-ray grating spectrometers,” *Proc. SPIE* **8147**, 81471L-1 (2011).
- [4] Mukherjee, P. *et al.*, “Plasma etch fabrication of 60:1 aspect ratio silicon nanogratings with 200 nm pitch,” *J. Vac. Sci. Technol. B* **28**, C6P70 (2010).
- [5] Bruccoleri, A. *et al.*, “Fabrication of nanoscale, high throughput, high aspect ratio freestanding gratings,” *J. Vac. Sci. Technol. B* **30**, 06FF03 (2012).
- [6] Bruccoleri, A. *et al.*, “Nanofabrication Advances for High Efficiency Critical-Angle Transmission Gratings,” *Proc. SPIE* **8861**, 886119 (2013).
- [7] Bruccoleri, A., Heilmann, R. K., and Schattenburg, M. L., “Fabrication process for 200 nm-pitch polished freestanding ultrahigh aspect ratio gratings,” *J. Vac. Sci. Technol. B* **34**, 06KD02 (2016).
- [8] Heilmann, R. K. *et al.*, “Critical-Angle X-ray Transmission Grating Spectrometer with Extended Bandpass and Resolving Power $> 10,000$,” *Proc. SPIE* **9905**, 99051X-1 (2016).
- [9] Dewey, D., Humphries, D. N., McLean, G. Y., Moschella, D. A., “Laboratory Calibration of X-Ray Transmission Diffraction Gratings,” *Proc. SPIE* **2280**, pp. 257-271 (1994).
- [10] Anderson, E. H. Levine, A. M., Schattenburg, M. L., “Transmission x-ray diffraction grating alignment using a photoelastic modulator,” *Appl. Opt.* **27**, 16 (1988).
- [11] Günther, H. M. *et al.*, “Performance of a double tilted-Rowland-spectrometer on ARCUS,” *Proc. SPIE* **10397** (paper 26), to be published (2017).
- [12] Ferrera, J., Schattenburg, M. L., Smith, H. I., “Analysis of distortion in interference lithography,” *J. Vac. Sci. Technol. B* **14**, 4009 (1996).
- [13] Walsh, M. E., Ph.D. Thesis, “On the design of lithographic interferometers and their application,” (2004).
- [14] Heilmann, R. K. *et al.*, “Critical-angle transmission grating technology development for high resolving power soft x-ray spectrometers on Arcus and Lynx,” *Proc. SPIE* **10399** (paper 39), to be published (2017).